SINGLE PHOTON SOURCES FOR QUANTUM CRYPTOGRAPHY AND QUANTUM COMPUTING

BY S. FRÉDÉRICK, D. DALACU, D. KIM, P. POOLE, G.C. AERS, AND R.L. WILLIAMS

The quantization of light can be viewed as the association of a quantized simple harmonic oscillator with each mode of the electromagnetic field. This association was made in the papers of Dirac [1] and Fermi [2] in response to works from Planck [3] and Einstein [4], which were themselves concerned with the ultraviolet catastrophe of the black body spectrum and the photoelectron effect respectively. A complete, modern treatment of the quantized radiation field can be found in Mandel and Wolf [5] and Scully and Zubairy [6] .One result of such a quantization is the description of the local electric field as a quantum mechanical operator, written in terms of harmonic oscillator creation and annihilation operators, $a^{+}_{\mathbf{ks}}$ and $a_{\mathbf{ks}}$, which create or remove a single quantum, or photon, from the electromagnetic field mode described by the wave vector **k** and polarization index s within an enclosure of volume V ;

$$\mathbf{E}(\mathbf{r},t) = \mathbf{E}^{(+)}(\mathbf{r},t) + \mathbf{E}^{(-)}(\mathbf{r},t)$$

$$\mathbf{E}^{(+)}(\mathbf{r},t) = \sum_{\mathbf{k},s} E^{0}_{\mathbf{k}} a_{\mathbf{ks}} \boldsymbol{\varepsilon}_{\mathbf{ks}} e^{i(\mathbf{k}\cdot\mathbf{r}-\omega_{\mathbf{k}}t)}$$

$$\mathbf{E}^{(-)}(\mathbf{r},t) = \sum_{\mathbf{k},s} E^{0}_{\mathbf{k}} a^{+}_{\mathbf{ks}} \boldsymbol{\varepsilon}_{\mathbf{ks}} e^{-i(\mathbf{k}\cdot\mathbf{r}-\omega_{\mathbf{k}}t)}$$

Here, $\boldsymbol{\varepsilon}_{\mathbf{k}1}$ and $\boldsymbol{\varepsilon}_{\mathbf{k}2}$ describe two orthogonal polarization states and $E^{0}_{\mathbf{k}} = \sqrt{\dfrac{\hbar\omega_{\mathbf{k}}}{2\varepsilon_0 V}}$ has the units of an electric field.

Within such a formalism, the possibility of Fock or number states arises, an example of which is given by the state of the electromagnetic field described by

$$|n\rangle = \frac{(a^{+}_{\mathbf{ks}})^{n}}{\sqrt{n!}}|0\rangle,$$

which corresponds to n quanta generated in the mode (**k**,s) by repeated application of the appropriate creation operator to the vacuum state. The state, $|0\rangle$, is a particular example of a number state, all be it a trivial one in which no photons are present. Apart from the vacuum state, the preparation and characterization of number states of the radiation field is extremely demanding. In this paper we discuss the preparation, characterization and application of number states of the radiation field, with particular emphasis on the construction of sources of single photons based on solid state nanostructures.

SUMMARY

Sources of single photons, their characterization and uses are reviewed with emphasis on solid state sources based on semiconductor nanostructures.

CORRELATION SPECTROSCOPY

A common form of optical characterization involves the annihilation of a photon from the radiation field following interaction with a detector. Typically such a process produces a charged particle that is counted as a means of measurement. For such a detector at position **r** in the radiation field, one can show [7] that the probability of detecting an event between time t and $t + dt$ is proportional to $w_I(\mathbf{r},t)dt$, where

$$w_I(\mathbf{r},t) = \langle i|\mathbf{E}^{(-)}(\mathbf{r},t)\cdot\mathbf{E}^{(+)}(\mathbf{r},t)|i\rangle$$

and $|i\rangle$ is the initial state of the radiation field.

A similar treatment can be applied to the case of two independent detectors placed at locations **r** and **r**′. The probability of detecting an event at **r**′ between time t' and $t' + dt'$, whilst detecting another at **r** between time t and $t + dt$ is proportional to $w_{II}(\mathbf{r},t,\mathbf{r}',t')dtdt'$, where

$$w_{II}(\mathbf{r},t,\mathbf{r}',t') = \langle i|\mathbf{E}^{(-)}(\mathbf{r}',t')\mathbf{E}^{(-)}(\mathbf{r},t)\mathbf{E}^{(+)}(\mathbf{r},t)\mathbf{E}^{(+)}(\mathbf{r}',t')|i\rangle$$

and we have assumed a linearly polarized electric field. If the radiation field is statistically invariant as a function of time, so that only the difference $\tau = t - t'$ is significant, then this leads us to define a normalized, second order quantum mechanical correlation function as a statistical average over all possible realizations of the initial field,

$$g^{(2)}(\mathbf{r},\tau) = \frac{\left\langle \mathbf{E}^{(-)}(\mathbf{r},t)\mathbf{E}^{(-)}(\mathbf{r},t+\tau)\mathbf{E}^{(+)}(\mathbf{r},t+\tau)\mathbf{E}^{(+)}(\mathbf{r},t)\right\rangle}{\left\langle \mathbf{E}^{(-)}(\mathbf{r},t)\mathbf{E}^{(+)}(\mathbf{r},t)\right\rangle\left\langle \mathbf{E}^{(-)}(\mathbf{r},t+\tau)\mathbf{E}^{(+)}(\mathbf{r},t+\tau)\right\rangle}$$

Classically, $g^{(2)}(\tau)$ can be written as

$$g^{(2)}{}_{classical}(\tau) = \frac{\langle I(t+\tau)I(t)\rangle}{\langle I(t)\rangle^{2}}$$

and the Cauchy-Schwartz inequalities,

$$g^{(2)}{}_{classical}(0) \geq 1$$

$$g^{(2)}{}_{classical}(0) \geq g^{(2)}{}_{classical}(\tau)$$

S. Frédérick[1,2] <Simon.Frederick@nrc-cnrc.gc.ca>; D. Dalacu[1] ; D. Kim[1,3] ; P. Poole[1] ; G.C. Aers[1] ; R.L. Williams[1,2,3]

[1] Institute for Microstructural Sciences, National Research Council of Canada, Ottawa, ON, K1A 0R6;
[2] Physics Department, University Of Ottawa, Ottawa ON 61N 6N5;
[3] Department of Materials Science and Engineering, University of Toronto, Toronto, ON M5S 3E4

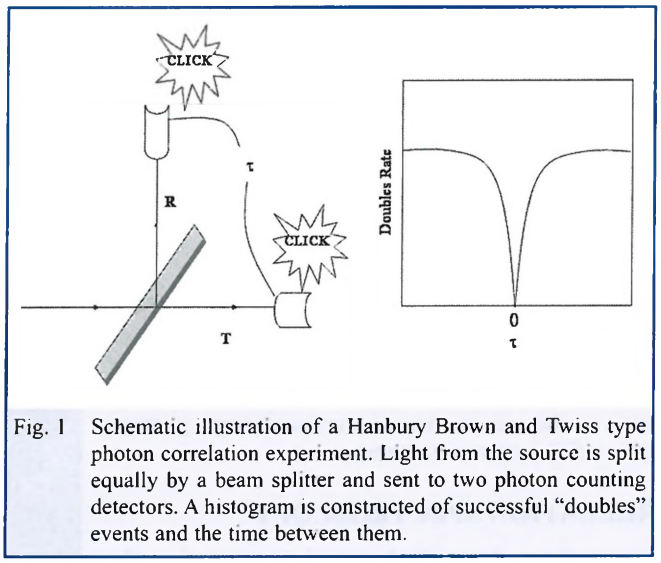

Fig. 1 Schematic illustration of a Hanbury Brown and Twiss type photon correlation experiment. Light from the source is split equally by a beam splitter and sent to two photon counting detectors. A histogram is constructed of successful "doubles" events and the time between them.

are obeyed. Such behavior is displayed for example by a classical thermal source and by the high intensity emission from a laser, in which the probability of finding n photons in the mode obeys a Poisson distribution [6]. For the quantum mechanical second order correlation function it is possible to obtain values for $g^{(2)}(0)$ lying between 0 and 1 and the photons are said to be *antibunched* – detecting a photon at one place and time makes it less likely to detect a second.

The quantum mechanical second order correlation function can be accessed experimentally by measuring the response of detectors placed in the two output arms of a 50:50 beamsplitter (Fig. 1). Such experiments were proposed by Hanbury Brown and Twiss [8] to study the coherence properties of radio stars and have developed as a valuable means to measure the statistical properties of non-classical states of light. In Figure 1 the use of such an arrangement to measure the statistics for a single photon emitter is illustrated. Classically, the 50:50 beam splitter in Figure 1 simply acts to split the wave front equally between reflection (R) and Transmission (T). If the incoming wave fluctuates, then positive correlations will be observed at the two detectors, $g^{(2)}(0) > 1$, whilst if the wave is perfectly stable then $g^{(2)}(0) = 1$. Quantum mechanically, for a single photon field, the observation of a "click" on one detector collapses the wavefunction to that particular arm of the system and no simultaneous ($\tau = 0$) "click" can be observed on the second detector, $g^{(2)}(0) = 0$. Such anti-correlation between the two detectors is a purely quantum effect and cannot be explained using a classical description of the field.

APPLICATIONS OF SINGLE PHOTON SOURCES

Quantum Cryptography

The distribution of cryptographic keys using demonstrably secure optical means has been one of the main motivational drives for the development of single photon sources. The earliest quantum key distribution protocol (BB84) was presented by Bennet and Brassard in 1984 [9] and is based upon two fundamental quantum mechanical principles; that it is not possible to clone an individual quantum state and that, unless in an eigenstate of the measurement operator, a measurement will inherently introduce a modification to the state that can be detected. Within the BB84 protocol, the quantum mechanical system in question is a single photon and quantum information is encoded within the photon's state of polarization. Under the assumption of ideal experimental conditions, with no limitations on the source, detectors etc. the quantum key distribution discussed in BB84 is absolutely secure. Details of the many variations to the initial BB84 protocol can be found in the literature [10-12] and detailed discussions are given elsewhere in this issue. Initial demonstrations of quantum key distribution systems used weak laser pulses as approximations to true single photon sources. However, the Poisson distribution of photon number within each pulse introduces the possibility of insecure key exchange if individual photons from multi-photon pulses can be examined with impunity. The first demonstrations of quantum key distribution using true single photon sources were performed by Beveratos *et al* in 2002 [13] using a Nitrogen-Vacancy pair source in diamond and by Waks *et al* also in 2002 [14] using a solid state nanostructure embedded within a microcavity.

Linear Optics Quantum Computation

In principle the single photon provides a very attractive realization of a quantum bit or "qubit". A coherent superposition of two polarization states of the photon, horizontal $|H\rangle$ or vertical $|V\rangle$, could be used to describe the general polarization state of a single qubit,

$$|\psi\rangle = \alpha|H\rangle + \beta|V\rangle$$

with the continuous complex variables α and β ($|\alpha|^2 + |\beta|^2 = 1$) being used to encode quantum information. Photons are attractive for quantum information applications because they interact very little with the environment and they can be easily transported between locations. However, photons also interact very little with each other unless highly non-linear materials are used and until recently this was seen as a major obstacle to the use of photons in quantum computing applications, where it is necessary to produce and transport entangled states of many photons, in which the multi-photon wavefunction cannot be factored into product states that describe individual photons. In the paper by Knill, Laflamme and Milburn (2001) however [15], a scheme was presented in which efficient, non-deterministic quantum computing could be achieved using only single photon sources and linear optical components such as beamsplitters and phase shifters. The only non-linear elements within the scheme are detectors. The price to pay for this capability was that the quantum gates used in the computer would not be successful at every attempt, but one would know when they had succeeded and could proceed accordingly. Since this initial proposal, further work [16] has shown how the resources required to implement two qubit gates can be drastically reduced.

Squeezed Light Measurements

For a single mode field, the electric field operator can be written as [6],

$$\mathbf{E}(t) = E^0\boldsymbol{\varepsilon}\left(ae^{-i\omega t} + a^+e^{i\omega t}\right)$$

where a,a^+ obey the commutation relation, $\lfloor a,a^+\rfloor = 1$. Introducing the two quadrature amplitude operators,

$$X_+ = \left(a + a^+\right)$$
$$X_- = -i\left(a - a^+\right)$$

we find

$$\mathbf{E}(t) = E^0\boldsymbol{\varepsilon}\left(X_+Cos\omega t + X_-Sin\omega t\right)$$

and identify X_+ and X_- as the amplitude of the two field quadratures. Given that the commutator between X_+ and X_- satisfies $[X_+, X_-] = 2i$, the Uncertainty Principle leads us to conclude that the uncertainties in the two quadratures are such that

$$\Delta X_+ \Delta X_- \geq 1$$

Light from a laser (approximated by a coherent state, having a Poisson distribution of photon number) or in the vacuum state, is such that the uncertainty in the two quadratures is equal and corresponds to a minimum uncertainty state i.e. $\Delta X_+ \Delta X_- = 1$. However, quantum mechanics allows states of the radiation field to be generated in which the uncertainty in one quadrature is reduced below the other and below that which is obtained in a symmetric, minimum uncertainty state, provided that the uncertainty product still obeys the Uncertainty Principle. Quadrature squeezed states open the possibility for noise reduced measurement and were first demonstrated by Wu *et al* [17]. Uses of such states include gravitational wave interferometery [18], measurements of nano-displacement [19] and atomic spectroscopy [20].

Single photon sources are not themselves quadrature squeezed states in the sense described above, but instead are amplitude or number squeezed, with corresponding increases in the phase uncertainty. As such it is possible to use single photon sources directly to reduce the amplitude noise in absorption spectroscopy [21] or indirectly in combination with linear optical elements as generators of entangled pairs, which can themselves be used for example in quantum lithography [22].

EXPERIMENTAL REALIZATION OF SINGLE PHOTON SOURCES

In this section we briefly discuss a number of potential single photon sources that have been investigated.

Nitrogen-Vacancy Pairs in Diamond

The Nitrogen-Vacancy defect in diamond consists of a substitutional nitrogen atom, with a nearest neighbor vacancy. Nitrogen impurities occur naturally in diamond or they can be added deliberately through implantation [23], whilst vacancies can be generated by electron or neutron bombardment [24]. A review of single defects in diamond can be found in [25]. The main optical signature of the Nitrogen-Vacancy pair is a strong zero phonon emission line at 637nm, which corresponds to transitions between two spin triplet ground and excited states. The non-classical nature of the light emission from the Nitrogen-Vacancy centre has been confirmed [26,27] through measurements of $g^{(2)}(0) \leq 1$.

The Nitrogen-Vacancy pair is a strong candidate for a room temperature single photon source, provided that one is not interested in fiber-based systems, where the wavelength of 637nm is not appropriate. Also there may be issues related to the presence of dark states that produce $g^{(2)}(\tau) > 1$ for long delays [26].

Spontaneous Parametric Down Conversion

Spontaneous parametric down conversion is the non-linear optical process in which a single incident photon is converted into two outgoing photons within a crystal having a non-zero second order non-linear susceptibility, $\chi^{(2)}$. Such crystals include Potassium Dihydrogen Phosphate (KDP), β-Barium Borate (BBO, BaB_2O_4) and Lithium Iodate ($LiIO_3$). The conversion of the incident photon into the two "signal" and "idler" photons is an extremely inefficient (10^{-10}), energy and wave vector conserving process that can be used as a source of "heralded" single photons [28]. In such a case, the detection of one emitted photon is used to project its partner into a single photon Fock state. Depending upon conditions, the parametric down conversion process can produce two photons of identical energy (degenerate down conversion) or widely different energies (non-degenerate down conversion). This behavior allows the possibility, for example, to use injected light in the visible (532nm) to produce down converted photons at 1550nm for fiber applications whilst using easily detected 810nm photons as heralds.

The major drawbacks with spontaneous parametric down conversion for use as a single photon source, are the poor efficiency, large bandwidth (typically tens of nanometers) and the lack of scalability – if one were interested in producing integrated arrays of single photon emitters for quantum computing applications.

Single Molecules

Electronic states within molecules are typically accompanied by a series of harmonic oscillator product states associated with phonons. Molecules in the ground electronic state can be excited directly to the ground vibrational level of the excited electronic state, or to any of the excited vibrational levels above this. At low temperature, for molecules that are of interest for single photon sources, electronically and vibrationally excited molecules quickly (~ picoseconds) relax to the vibrational ground state. This quick relaxation allows an efficient preparation of the molecule into the excited state required for single photon emission.

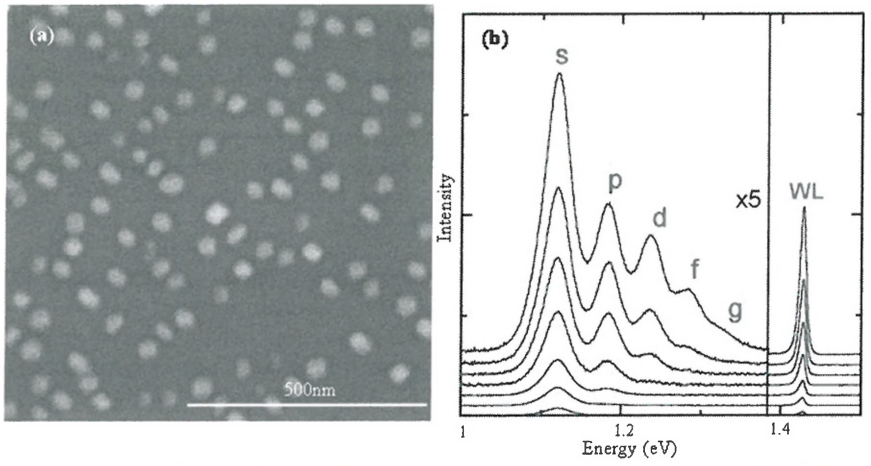

Fig. 2 (a) SEM micrograph showing randomly distributed InAs self-assembled quantum dots. (b) Photoluminescence emission from an ensemble of InAs quantum dots within a GaAs matrix. A series of seven spectra taken at increasing levels of optical excitation show development of quantum dot shell structure – s, p, d, f, g. The peak labeled "WL" corresponds to emission from the two-dimensional wetting layer on which the dots are formed.

Although single photon antibunching has been demonstrated in molecular systems at both room temperature and liquid helium temperatures [29], a major drawback of these systems tends to be their limited stability, with photochemical processes destroying the emitting molecules within minutes to hours.

Self-Assembled Quantum Dots

The deposition of compressively strained overlayers onto a semiconductor substrate can, under the appropriate conditions, result in a growth mode in which three-dimensional islands are nucleated spontaneously after a few monolayers of normal, layer by layer growth. This Stranski Krastanow [30] growth mode has been used to produce lower bandgap semiconductor "quantum dots" or "quantum boxes", surrounded by a higher bandgap semiconductor matrix. The self-assembled quantum dots produced in this manner result in full, three-dimensional quantization of the energy states of trapped charges and excitonic complexes and are of great interest for applications in quantum information processing and next generation optical and electronic devices [31,32]. At low temperatures, under weak excitation, an emission linewidth corresponding to the excitonic radiative lifetime has been observed [33,34]. An example of a quantum dot ensemble produced spontaneously during growth, along with a typical luminescence emission spectrum for an InAs quantum dot ensemble within a GaAs matrix is shown in Figure 2. From the scanning electron microscope image in Figure 2(a), it is clear that there exists a large variation in quantum dot size, shape and orientation. To a certain extent, it is this ability to change the size and shape of individual quantum dots that makes them particularly interesting for quantum information applications, since it gives one the ability to engineer the precise optical properties and electrical configuration needed for a particular application. In ensemble optical measurements however, it is this variation that is responsible for the inhomogeneous broadening of the emission that masks the behavior of individual dots.

For fiber-based quantum cryptography applications, single photons in the wavelength regions around 1300nm and 1550nm are preferred. Although they can be produced with emission wavelength around 1300nm [35], typical InAs/GaAs dots are found to emit at wavelengths around 1μm. For 1550nm and also around 1300nm, InAs quantum dots within in an InP matrix are preferred [36]. In Figure 3 we show luminescence emission from a single InAs/InP quantum dot at low temperature. Isolation of an individual dot is achieved by etching mesas into a low density, quantum dot ensemble and then searching for the small number of mesas that show single dot emission behavior.

In a similar manner to single InAs/GaAs quantum dots, the low temperature emission evidenced in Figure 3 corresponds to a series of sharp lines representing the annihilation of a single electron-hole pair in the presence of a variable number of "spectator" charges depending on the level of optical excitation. At the lowest level of excitation, the optical emission corresponds to the recombination of a single interacting electron-hole pair, or exciton, residing in the s-shell of the quantum dot. It is this recombination event that has been pursued as the source of triggered single photons [37].

To provide an efficient source of single photons based on single self-assembled quantum dots, it is desirable to couple the

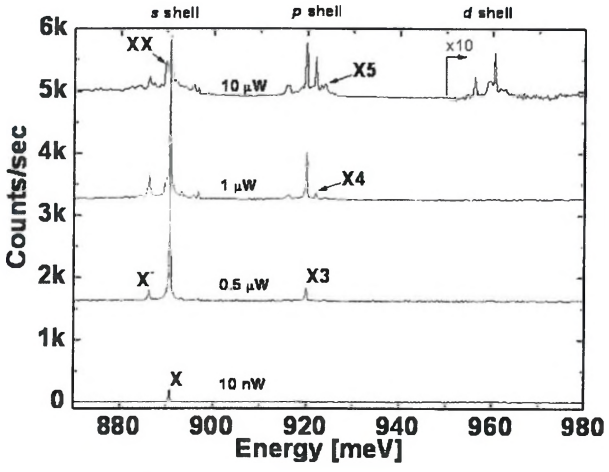

Fig. 3 Photoluminescence emission at increasing levels of optical pump power for an individual InAs/InP quantum dot isolated within an etched mesa.

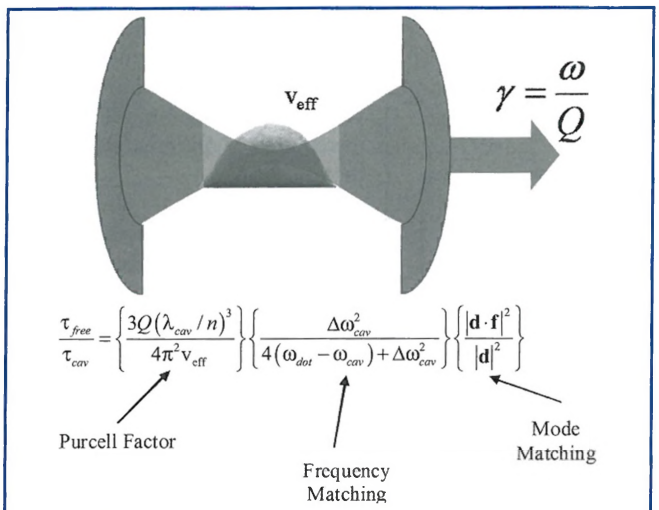

Fig. 4 Schematic illustration showing the matching of a low loss cavity of mode volume v_{eff} to the excitonic emission of a single, self-assembled quantum dot. The cavity is characterized by a photon loss rate $\gamma = \frac{\omega}{Q}$, where Q is the cavity quality factor.

ground state, excitonic transition to the optical mode of a low loss microcavity, as shown schematically in Figure 4.

In the weak coupling regime, where the dominant decoherence process is photon loss through the cavity mirrors, this coupling to the cavity will produce an enhancement of the spontaneous emission rate given by the Purcell factor [38], provided that (i) the cavity frequency and quantum dot transition frequency are matched and (ii) the quantum dot dipole, **d**, is matched in both location and orientation to the cavity mode field distribution, **f**. Construction of an efficient single photon source based on single quantum dots can be viewed then as maximizing the ratio $\frac{Q}{v_{eff}}$ for a particular choice of cavity type, whilst simultaneously tuning the cavity mode frequency to match the selected dot transition and locating the appropriately oriented quantum dot at the anti-node of the cavity electric field distribution. To date, photon anti-bunching has been demonstrated in the low temperature emission from isolated quantum dots [39] in the absence of a cavity and from dots in various types of optical cavity [40], where alignment of the dot to the cavity mode is left purely to chance.

To go beyond structures in which dot alignment is left to chance, one must consider techniques for controlling the nucleation site of individual dots. Such a capability would allow not only the reproducible fabrication of efficient single photon emitters, but also the coupling of multiple, spatially separated quantum dots through interaction with a single microcavity optical mode; a capability that is of great interest for quantum computing applications. Control of quantum dot nucleation site can be achieved by controlling the movement of deposited quantum dot material, InAs, on the substrate surface during epitaxial growth [40]. Once deposited, if InAs can be persuaded to migrate to a particular location, then strain-induced nucleation of dots will result. In Figure 5, we show one technique for producing such "site-selected" quantum dots. Here, an InP nanotemplate having {110} sidewalls and a [001] top surface is produced in-situ during crystal growth by patterning the substrate surface with a dielectric mask and opening up "windows" of the appropriate geometry. Growth on such a surface occurs only within the windows, to produce clean InP templates that can be used subsequently to control the surface motion of deposited InAs.

Quantum dot material deposited on these templates is found to migrate away from the {110} surfaces, to accumulate on the [001] top surface, where dots are nucleated. Figure 5(b) and (c) show the nucleation of a single dot and a linear dot chain on templates with "pyramidal" and "stripe" geometry respectively. Once nucleated, the InAs dots can be capped with InP in the normal way to produce, clean, luminescently efficient dots with known location [42]. In addition, if the surrounding dielectric mask is removed, a second InP growth step can be used which planarises the structure, to produce a thin (~300nm) InP layer with a single embedded InAs quantum dot.

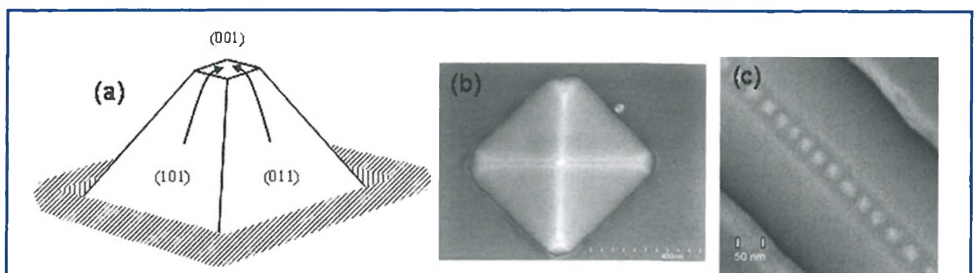

Fig. 5 (a) Schematic illustration of an InP, square-based, pyramidal nano-template used for the site-selective growth of single InAs quantum dots. (b) Scanning electron micrograph of a single InAs quantum dot nucleated at the apex of a nanotemplate. (c) Linear array of coupled quantum dots nucleated at the apex of a "stripe" geometry nanotemplate.

Using the site-selection and planarisation technique described above, it is now possible to build optical cavities that are matched to the measured location, polarization and transition frequency of the dot. In Figure 6 we show one example of such a cavity; the pillar microcavity. The cavity mirrors, both above and below the quantum dot layer, are multiple quarter-wavelength pairs of high and low index material, in this case SiO_2 and Ta_2O_5. An optical cavity, with an electric field antinode at the centre, is formed by separating the mirrors by one half of a wavelength [43].

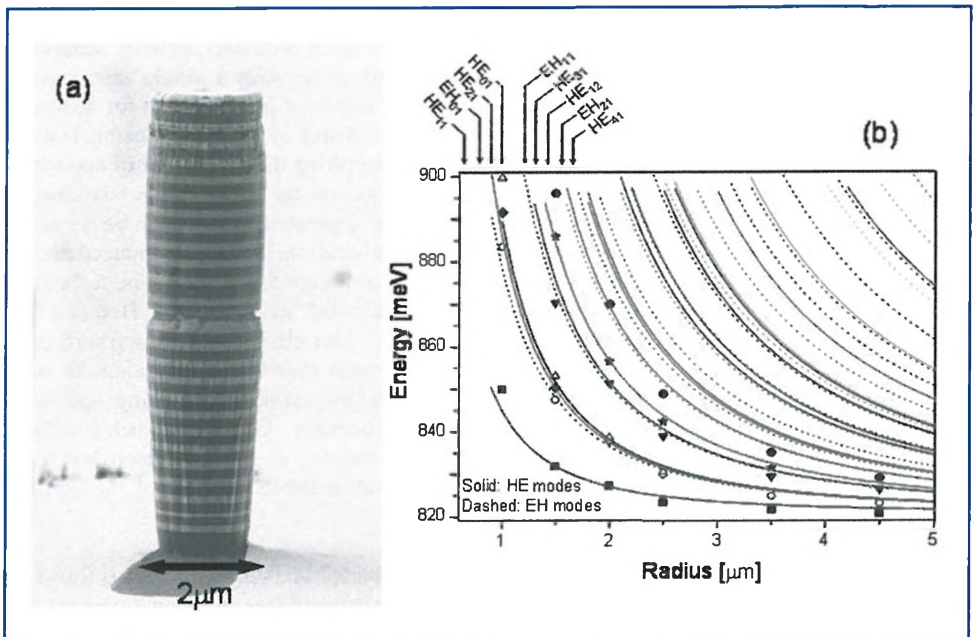

Fig. 6 (a) Scanning Electron Micrograph of a SiO2/Ta2O5 pillar microcavity. (b) Experimental (symbols) and calculated (lines) mode energies of the pillar microcavity as a function of pillar radius.

Figure 6(b) shows how the mode structure of these types of cavity can be tuned by etching pillars of a particular radius. In principle then, once the dot emission energy is known, a pillar cavity of the appropriate radius can be etched to match it. Unfortunately, this etching procedure is difficult to iterate, so that unless the pillar dimension is chosen correctly the first time, it is difficult to correct. In addition, the etching process itself produces roughness on the pillar surface, so that the cavity Q is reduced for smaller radii. Although wide cavities can be produced with Qs of a few thousand, the Q drops to below 500 for radii of the order of 500nm. As a consequence, it is difficult to produce a high Q pillar cavity with a small mode volume, as required to optimize the Purcell factor.

To produce small mode volume and high Q simultaneously, it is advantageous to work with two-dimensional photonic crystal, optical defect microcavities such as that shown in Figure 7.

Such cavities are based on total internal reflection within a thin semiconductor membrane and, as such, are ideally suited to the planarised, single quantum dot process discussed above.

Within the membrane plane, periodic dielectric contrast can be achieved by etching a series of through-holes, and the resulting Bragg reflection used to engineer a strongly localized, high Q photonic mode [44]. A hexagonal symmetry, single missing hole defect cavity, with x- and y-dipole modes is shown in Figure 8.

Finite difference time domain modeling of cavities such as these predict a Q value in excess of 80,000 and a corresponding mode volume of approximately $0.5(\lambda/n)^3$, where "n" is the refractive index of the cavity membrane. In GaAs based cavi-

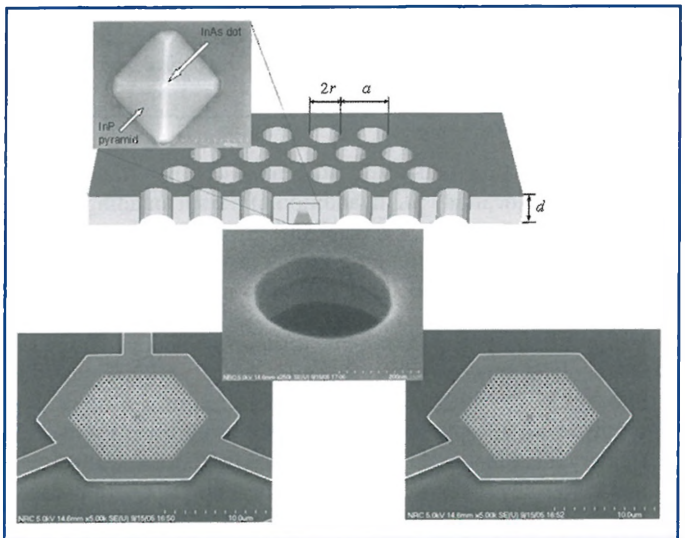

Fig. 7 Schematic illustration and scanning electron micrographs of InP, photonic crystal microcavity membranes based on planarised, site-selected quantum dots.

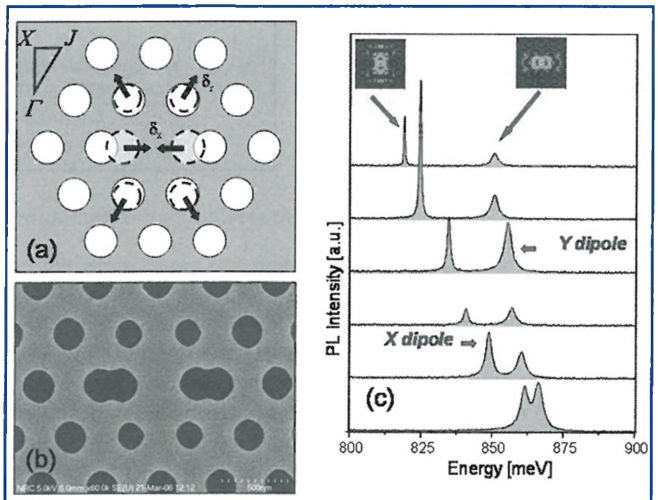

Fig. 8 (a) Geometry perturbations used to optimize the Q of the x-dipole mode in single missing hole defect cavities. (b) Scanning electron micrograph of an optimized x-dipole cavity. (c) Emission characteristics for a variety of single missing hole defect cavities showing optimization of the Q of the x-dipole mode.

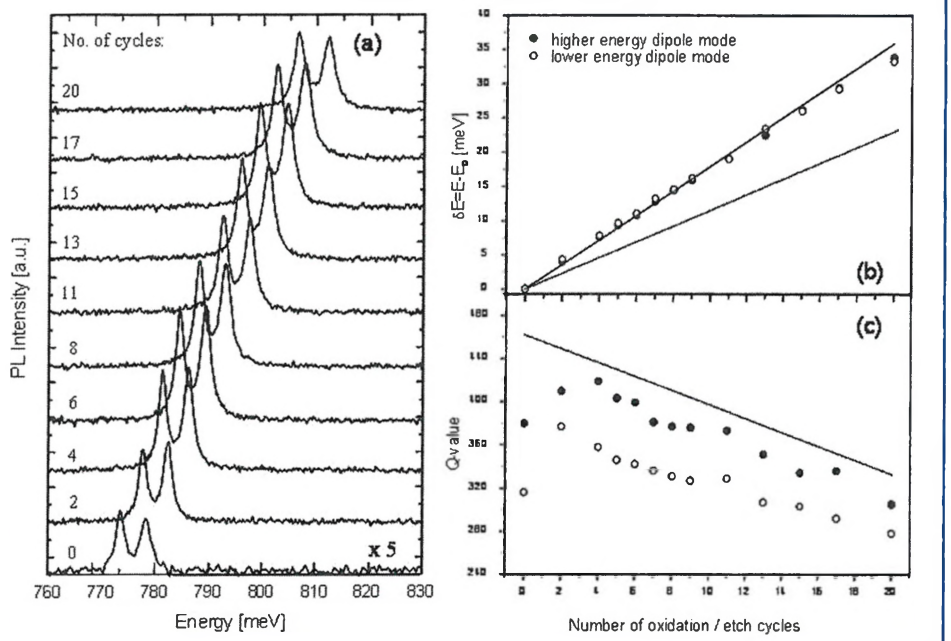

Fig. 9 (a) Energy tuning of the x- and y-dipole modes of a single missing hole defect photonic crystal microcavity through repeated etch and oxidation cycles. (b) Energy shift and (c) Q value per cycle of oxidation and etch.

ties of this type, Q values of approximately 5,000 have been reported experimentally [45], whilst Q > 28,000 has been reported in InP cavities [46].

In addition to the advantages of high Q and small mode volume presented by photonic crystal microcavity membranes, these cavities also allow tuning of the cavity mode frequency to match the transition energy of an embedded quantum dot, as shown in Figure 9.

In this process, the photonic crystal cavity is oxidized using a UV-ozone treatment; converting a fraction of the InP membrane surface and the inner surface of the etched holes into oxides of InP [47]. The removal of the generated oxide using wet chemical processing serves to widen the etched through-holes and reduces the membrane thickness, so shifting the modes to higher energy. Because the oxidation process is self-limiting, the oxidation/etch cycle produces step-wise, digital shifts in the mode energy of approximately 1.74meV per cycle.

REFERENCES

1. P.A.M. Dirac, *Proc. Roy. Soc. A* **114**, 243 (1927).
2. E. Fermi, *Rev. Mod. Phys.* **4**, 87 (1932).
3. M. Planck, *Verh. Deutsch. Phys. Ges.* **2**, 202 (1900).
4. A. Einstein, *Ann. Phys.* **17**, 132 (1905).
5. L. Mandel and E. Wolf, *Optical Coherence and Quantum Optics,* Cambridge University Press, (1995).
6. M.O. Scully and M.S. Zubairy, *Quantum Optics,* Cambridge University Press, (1997).
7. R.J. Glauber, *Phys. Rev.* **130**, 2529 (1963).
8. R. Hanbury Brown and R.Q. Twiss, *Nature* **177**, 27 (1956).
9. C.H. Bennett and G. Brassard, *Proceedings of the International Conference on Computer Systems and Signal Processing*, Bangalore, p.175 (1984).
10. D. Gottesman and J. Preskill, *Phys. Rev. A* **63**, 022309 (2001).
11. Ch. Silberhorn, N. Korolkova, G. Leuchs, *Phys. Rev. Lett*, **88**, 167902 (2002).
12. F. Grosshans, G. Van Assche, J. Wenger, R. Brouri, N.J. Cerf, and Ph. Grangier, *Nature* **421**, 238–241 (2003).
13. A. Beveratos, R. Brouri, T. Gacoin, A. Villing, J-P. Poizat and Ph. Grangier, *Phys. Rev. Lett.* **89**, 187901 (2002).
14. E. Waks, K. Inoue, C. Santori, D. Fattal, J. Vuckovic, G.S. Solomon, Y. Yamamoto, *Nature* **420**, 762 (2002).
15. E. Knill, R. Laflamme and G.J. Milburn, *Nature* **409**, 46 (2001).
16. N. Yoran and B. Reznik, *Phys. Rev. Lett.* **91**, 037903 (2003).
17. L-A. Wu, H.J. Kimble, J.L. Hall, H. Wu, *Phys. Rev. Lett.* **57**, 2520 (1986).
18. T. Corbitt and N. Mavalvala, *J. Opt. B: Quantum Semiclass. Opt.* **6**, S675 (2004) .
19. N. Treps, N. Grosse, W.P. Bowen, M.T.L. Hsu, A. Maître, C. Fabre, H-A. Bachor and P.K. Lam, *J. Opt. B: Quantum Semiclass. Opt.* **6**, S664 (2004) .
20. E.S. Polzik, J. Carri, and H.J. Kimble, *Appl. Phys. B* **55**, 279 (1992).
21. B. Lounis and M. Orrit, *Rep. Prog. Phys.* **68**, 1129 (2005).
22. P. Kok, S.L. Braunstein and J.P. Dowling, *J. Opt. B: Quantum Semiclass. Opt.* **6**, S811 (2004).
23. J. Meijer, B. Burchard, M. Domhan, C. Wittmann, T. Gaebel, I. Popa, F. Jelezko and J. Wrachtrup, *Appl. Phys. Lett.* **87**, 261909 (2005).

24. Y. Mita, *Phys. Rev. B* **53**, 11360 (1996).
25. F. Jelezko and J. Wrachtrup, *phys. stat. sol. (a)* **203**, 3207 (2006).
26. C. Kurtsiefer, S. Mayer, P. Zarda and H. Weinfurter, *Phys. Rev. Lett.* **85**, 290 (2000).
27. R.J. Epstein, F.M. Mendoza, Y.K. Kato and D.D. Awschalom, *Nature Physics* **1**, 94 (2005).
28. C.K. Hong and L. Mandel, *Phys. Rev. Lett.* **56**, 58 (1986).
29. B. Lounis and W.E. Moerner, *Nature* **407**, 491 (2000).
30. I.N. Stranski and Von L. Krastanow, *Akad. Wiss. Lit. Mainz Math.-Natur. Kl. IIb* **146**, 797 (1939).
31. M. Korkusinski, P. Hawrylak, *Phys. Rev. B* **63**, 195311 (2001).
32. G.W. Bryant, *Phys. Rev. B* **37**, 8763 (1988).
33. M. Bayer, A. Forchel, *Phys. Rev. B* **65**, 041 308 (2002).
34. C. Kammerer, C. Voisin, G. Cassabois, C. Delalande, Ph. Roussignol, F. Klopf, J.P. Reithmaier, A. Forchel, J.M. Gerard, *Phys. Rev B.* **66**, R041 306 (2002).
35. D.L. Huffaker and D.G. Deppe, *Appl. Phys. Lett.* **73**, 520 (1998).
36. P.J. Poole, J.P. McCaffrey, R.L. Williams, J. Lefebvre,and D. Basnagge, *J. Vac. Sci. Technol. B* **19**, (2001).
37. C. Santori, M. Pelton, G. Solomon, Y. Dale, and Y. Yamamoto, *Phys. Rev. Lett.* **86**, 1502 (2001).
38. E.M. Purcell, *Phys. Rev.* **69**, 681 (1946).
39. C. Becher, A. Kiraz, P. Michler, A. Imamoglu, W.V. Schoenfeld, P.M. Petroff, Lidong Zhang, E. Hu, *Phys. Rev. B* **63**, 121312(R) (2001).
40. P. Michler, A. Kiraz, C. Becher, W.V. Schoenfeld, P.M. Petroff, L. Zhang, E. Hu, A. Imamoglu, *Adv. Solid State Phys.* **41**, 3 (2001) (Springer, Berlin, Heidelberg 2001).
41. J. Lefebvre, P.J. Poole, J. Fraser, G.C. Aers, D. Chithrani and R.L. Williams, *J. Cryst. Growth*, **234**, 391 (2002).
42. D. Chithrani, R.L. Williams, J. Lefebvre, P.J. Poole, and G.C. Aers, *Appl. Phys. Lett.*, **84**, 978 (2004).
43. D. Dalacu, D. Poitras, J. Lefebvre, P.J. Poole, G.C. Aers, and R.L. Williams, *Appl. Phys. Lett.*, **84**, 3235 (2004).
44. D. Dalacu, S. Frédérick, A. Bogdanov, P.J. Poole, G.C. Aers, R.L. Williams, M.W. McCutcheon and J.F. Young, *J. Appl. Phys.*, **98**, 023101 (2005).
45. D. Englund, D. Fattal, E. Waks, G. Solomon, B. Zhang, T. Nakaoka, Y. Arakawa, Y. Yamamoto and J.J.Vučković, *Phys. Rev. Lett.* **95**, 013904 (2005).
46. S. Frédérick, D. Dalacu, J. Lapointe, P.J. Poole, G.C. Aers and R.L. Williams, *Appl. Phys. Lett.*, **89**, 091115 (2006).
47. D. Dalacu, S. Frédérick, P.J. Poole, G.C. Aers, and R.L. Williams, *Appl. Phys. Lett.*, **87**, 151107 (2005).